Obstructed atomic insulators with robust corner modes

Da-Shuai Ma [1,2] Kejun Yu,[3,4] Xiao-Ping Li [5] Xiaoyuan Zhou,[2,*] and Rui Wang [1,2,†]

[1]*Institute for Structure and Function & Department of Physics & Chongqing Key Laboratory for Strongly Coupled Physics,*
Chongqing University, Chongqing 400044, People's Republic of China
[2]*Center of Quantum materials and devices, Chongqing University, Chongqing 400044, People's Republic of China*
[3]*Centre for Quantum Physics, Key Laboratory of Advanced Optoelectronic Quantum Architecture and Measurement (MOE),*
School of Physics, Beijing Institute of Technology, Beijing 100081, China
[4]*Beijing Key Lab of Nanophotonics and Ultrafine Optoelectronic Systems, School of Physics,*
Beijing Institute of Technology, Beijing 100081, China
[5]*School of Physical Science and Technology, Inner Mongolia University, Hohhot 010021, China*

Higher-order topological insulators (HOTIs), that are classified as obstructed atomic insulators (OAIs) in the topological quantum chemistry (TQC) theory, attract great interest owning to the lower-dimensional topological boundary states. However, the boundary states in HOTIs reported so far are often fragile, manifested as strongly depending on crystalline symmetries and cleavage terminations in the disk or cylinder geometry. Here, using the TQC theory, we propose an intuitive strategy to establish the connection between the obstructed Wannier charge centers of OAIs and the emergence of robust corner states in two-dimensional systems. Based on first-principles calculations and real space invariant theory, we extend the concept of OAIs to phonon systems and thereby predict that the robust corner states can be realized in the phonon spectra of MX_3 (M = Bi, Sb, As, Sc, Y; X = I, Br, Cl) monolayers. The phonon corner modes in different shapes of nanodisks are investigated, and their robustness facilitates the detection in experiments and further applications. This work suggests a promising avenue to explore more attractive features of higher-order band topology beyond the existing paradigm.

Introduction.— The extension of quantized electric polarization from dipole moments to multipole moments has led to intense recent studies of higher-order topological insulators (HOTIs) [1]. The topological feature of HOTIs is characterized by nontrivial boundary states whose dimensionality is more than one below that of the bulk [2–12], i.e., a HOTI in d spatial dimensions possesses gapless boundary states at its $(d − n)$-dimensional boundaries ($n > 1$). The brand new bulk-boundary correspondence of HOTIs has enriched the community of topological states or materials and thus attracted intensive attention. Among various phases of HOTIs, of particular importance is the two-dimensional (2D) second-order topological insulator where spatial distribution of in-gap modes is localized at the corners of its 0D nanodisk [12–18]. The topological invariant and the robustness (under perturbations) of corner modes are well discussed [19–21]. In sharp contrast to the helical surface states in traditional topological insulators (TIs) [22], these characteristic corner modes are separated from the conduction bands and valence bands with the corresponding energy level adjustable by surface potential, leaving more freedom to detect them by spectroscopy experiments or be potentially applied in low-dimensional devices.

Different from searching traditional first-order topological materials, the systematic discovery of HOTIs is in its infancy. Fortunately, the symmetry-protected topological phase is well understood presently [23–26], which leaves the revealing of symmetry-protected HOTI to be accessible. Remarkably, topological quantum chemistry (TQC) theory [24,26] achieves great success in discovering nontrivial band topology. In the TQC theory, a system with nonzero real space invariant (RSI) [27,28] at empty Wyckoff positions (WPs) while the band representation (BR) is a sum of elementary band representations (EBRs) is a HOTI [28–30]. Equivalently, the HOTI can be diagnosed by checking whether the system is an obstructed atomic insulator (OAI) where the obstructed Wannier charge centers (OWCCs) mismatch with the occupied WPs. When a 2D OAI is clipped into 0D nanodisk where the OWCCs are exposed, the in-gap corner states would be accordingly present. While relevant advancements have been very encouraging, the presence of corner states in the 2D HOTIs reported so far strongly depends on the clipping geometries (i.e., crystalline symmetries and terminated atoms of nanodisks) [10,12,31–34], thus making it difficult for their experimental measurements or further practical applications. As corner states are the most interesting features of higher-order band topology in two dimensions, the exploration of HOTI candidates with robust corner states that are independent of the clipping forms is highly desirable.

On the other hand, it is also worth noting that the spin-orbit coupling is *not* a necessary condition for the presence of OAIs, indicating that the OAI can be realized in bosonic systems, such as photonic systems [35–38], acoustic systems [39–42],

*xiaoyuan2013@cqu.edu.cn
†rcwang@cqu.edu.cn

and electric circuits [43–45]. Therefore, since the first-order phononic topological insulator is nearly impossible to occur in realistic materials, it is expected to find phononic OAIs with HOTI features. In fact, the phonon in crystalline solids also works as another fancy platform for exploring nontrivial band topology and the related applications [46–57]. However, the OAI and its fascinating properties are rarely reported in phonon systems. Therefore, one would employ the theory of TQC to find materials with phononic higher-order band topology beyond the electronic materials.

In this work, we first elucidate the physical mechanism that the robust corner modes can emerge in 2D OAIs. Here, "robust" indicates that the emergence of corner state is independent of the clipping form of samples and the geometry of clipped nanodisks. We explain that such a unique feature is classified to the HOTI phase, which can be understood as an intuitive argument how *orbitals* locate at empty WPs. Then we adopt the theory of TQC to diagnose phonon band topology and search phononic OAIs in crystalline materials. Moreover, based on first-principles calculations and RSI theory, we show that the phononic OAIs with robust corner states that are not dependent on the clipping forms of nanodisks can be realized in the MX_3 (M = Bi, Sb, As, Sc,Y; X = I, Br, Cl) monolayers. Using the TQC theory, we find that the band topology of any odd number of phonon branches in these candidates is not equivalent to a conventional atomic insulator. Phonon orbitals locating at empty WPs $1a$ and $6i$ are validated, indicating the emergence of HOTI phase with robust corner states.

OAIs with robust corner modes.— As extensions of Su-Schrieffer-Heager model in higher dimensions, the corner modes emerge in kagome-3, breathing kagome, and pyrochlore lattices where the band gaps are in the OAI phase [31,58]. Nevertheless, for such OAIs, the corner modes are usually *fragile*, which means that the emergence of corner modes is strongly dependent on the clipping forms. For the kagome-3 lattice, shown in Fig. 1, when the lattice is clipped into a 0D nanodisk, the in-gap modes can only be found for corners with the exposed OWCC locating at the $1a$ (0,0) position, such as the Corner-I highlighted in blue in Fig. 1(a). Serving as a contrast to Corner-I, the OWCC is unexposed for Corner-II in Fig. 1(a), and there is no in-gap mode. Here, we claim for the first time that for a 2D OAI, if all of potentially exposed WPs are occupied by effective OWCCs, the corner modes would be robust and thus can be present in an arbitrary clipping form. For a kagome-3 lattice, the $3c$ ($\frac{1}{2}$, $\frac{1}{2}$) and $1a$ positions are respectively occupied by atoms and OWCC, while the $2b$ ($\frac{1}{3}$, $\frac{2}{3}$) position is empty. This is exactly the reason why the corner modes in this lattice are fragile. Serving as a contrast, as shown in Fig. 1(b), we here assume that an additional orbital acting as an OWCC is pinned at the $2b$ position. As a consequence, any kind of corner will expose the OWCC, and thus we can always obtain the corner modes that are robust and independent of the clipping form of the sample and the symmetries survived in the clipped nanodisks. In the main text, we reveal that such robust corner modes can be realized in the phonon spectra of MX_3 monolayers, forming unique phononic OAIs with attractive HOTI features. One should note that the freedom of spin is not a concern of this intuitive strategy. Thus, such robust corner modes
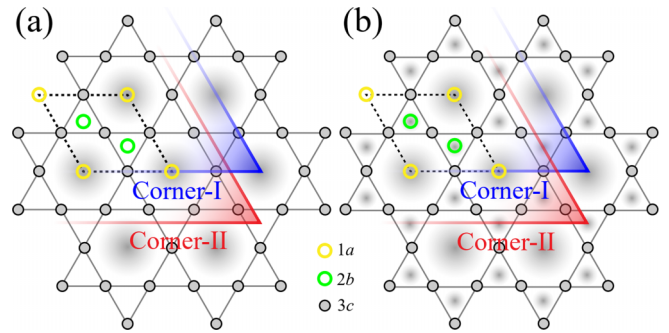

FIG. 1. (a) The schematic diagram of a kagome-3 lattice in which a set of *orbitals*, i.e., symmetric exponentially decayed Wannier functions are pinned at maximal WP $1a$. The second- and third-nearest-neighbor couplings are not shown. There are two kinds of corners, i.e., Corner-I (in blue) with the OWCC exposed and Corner-II (in red) with the OWCC unexposed. (b) Corresponding plots to panel (a) with an additional orbital pinned at $2b$. In panel (b), the OWCC will be exposed in both Corner-I and Corner-II. In both panels, WPs $1a$, $2b$, and $3c$ are represented by the circle in yellow, green, and black, respectively.

could be found in both bosonic and fermionic systems. In the Supplemental Material (SM) [59], we propose the As-Sb-As heterojunction is one of fermionic candidates.

Lattice structure of MX_3 monolayers.— Most recently, a new family of 2D layered semiconductor, i.e., the MX_3 monolayers, are synthesised experimentally [60]. The MX_3 monolayers crystallize in a hexagonal lattice with space group $P\bar{3}1m$ (No. 162) whose generators are inversion symmetry P, threefold rotational symmetry C_{3z}, and mirror symmetry M_{120}. The WPs $2c$ (1/3, 2/3, 0) and $6k$ (x, 0, z) are occupied by the metallic atoms M and halogen atoms X, respectively. As shown in Fig. 2(a), in MX_3 monolayers, each M atom is surrounded by six X atoms that are connected with each other by P and C_{3z}. Here, we take BiI_3 as an example and obtain the optimized lattice constant $a = 7.83$ Å, the nearest-neighbor Bi-I distance $d = 3.12$ Å, and the angle between Bi-I bond and the direction normal to the plane $\theta = 54.26°$, schematically shown in Fig. 2(b), through structural optimization. We tabulate the lattice parameters of MX_3 monolayers and experimental values of corresponding bulk structure in Table S1 in the SM [59]. The optimized parameters are in good agreement with the experimental values.

Phonon spectra of MX_3 monolayers.— In the main text, we mainly focus on the BiI_3 monolayer, and the results of other candidates are included in the SM [59]. The calculated phonon spectrum of BiI_3 monolayer is shown in Fig. 2(c). Originating from eight atoms per unit cell, there are 24 phonon branches, labeled as $PB_{k=1,2,\cdots,24}$, ordered by frequency from 0 THz to ~4.3 THz. It is found that all of the 24 branches can be divided into five sets by four visible phonon band gaps. Moreover, there are two sets of branches between 2.0 THz and 3.4 THz, as highlighted in red and blue in Fig. 2(c). Each set contains the unique quadruple-branch structure along the high-symmetry path Γ-M-K-Γ, similar to hourglass fermions [61], i.e., two double-degenerated points at Γ give rise to a branch-switching pattern along this path. Taking the set of red
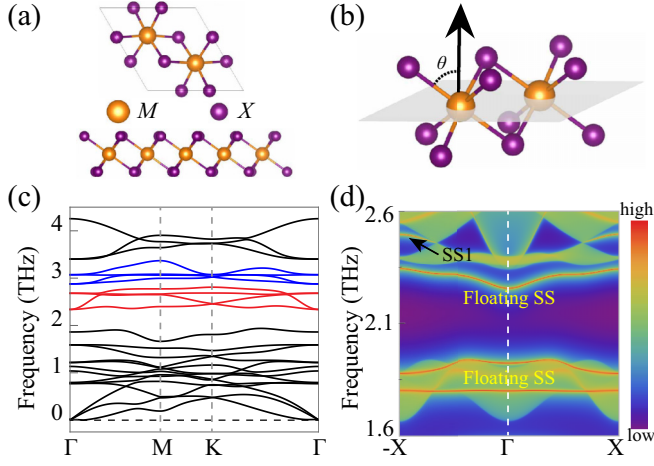
FIG. 2. The structure of MX_3 monolayers, and phonon spectrum and surface state of BiI$_3$ monolayer. (a) The top and side views of MX_3 monolayers. (b) The schematic diagram of the definition of the structure parameter θ, i.e., the angle between the M-X bond and the direction normal to the plane. (d) The calculated phonon spectrum of BiI$_3$ monolayer. Two special sets of bands formed by $PB_{14} \sim PB_{17}$ and $PB_{18} \sim PB_{21}$ (between 2.0 THz and 3.4 THz,) are highlighted in red and blue, respectively. (e) The projected edge states along the zigzag direction of BiI$_3$ monolayer. The SS1 connect the two projected Dirac points, and floating SSs are observed.

FIG. 3. (a) The schematic diagram of BiI$_3$ monolayer with a E_u *orbital* at 1a. The 6i position where a B orbital is located at is represented by the dots in white. The black dashed line marks the zigzag direction edge where the OWCCs are exposed. (b) The projected edge states along the zigzag direction of BiI$_3$ monolayer. (c) The phonon spectrum for a hexagonal-shaped nanodisk. The corner, edge, and bulk states are marked in red, blue, and black, respectively. The spatial distribution of the corner and edge phonon modes are shown as the inserts. (d) Corresponding plot to panel (c) starting from the triangular-shaped nanodisk.

phonon branches in Fig. 2(c) as an example, the quadratic branch dispersion at Γ and the linear branch crossing at K point appear near 2.4 THz. Noteworthy, as an analogy of that in graphene, the band topology of the linear Dirac point at K point implies that there is edge states connecting the projections of two gapless points. To verify this, we compute the phonon edge spectrum with an open boundary condition along the zigzag direction. As marked by SS1 in Fig. 2(d), the expectant edge state is obtained. Remarkably, in addition to the SS1 originating from the Dirac point, there are three other floating edge states, which is different from the 2D $\mathbb{Z}_2$ TI where the edge states connect the valence and conduction bands.

Filling-enforced OAI in MX_3 monolayers.— Here, we use the theory of TQC to diagnose the band topology and its novel properties in the phonon spectra of MX_3 monolayers. We calculated the representations of phonon branches at the maximal k vectors (see the SM [59]). We find that, for each of the four gaps, the BR can be written as a sum of EBRs, indicating these gaps are in atomic insulator or OAI phases, i.e., are identified as *trivial* insulators by TQC. Then, we give a brief introduction of filling-enforced OAI (feOAI) to reveal the phononic OAI phase. Without loss of generality, we assume a system belongs to space group G, and the WPs $(\omega_1, \omega_2, \cdots, \omega_M)$ are occupied. The site symmetry of the ω_i WP is g_{ω_i}, and the jth irreducible representations (Irrps) of g_{ω_i} are $\rho_{\omega_i}^{j=1,2,\cdots,N_{rep,\omega_i}}$. According to the theory of TQC, the Irrps $\rho_{\omega_i}^j$ in space group G can be expressed as $\rho_{\omega_i}^j \uparrow G$. The corresponding dimension is denoted as $d(\rho_{\omega_i}^j \uparrow G)$. In this case, for a trivial insulator the necessary and sufficient conditions for a
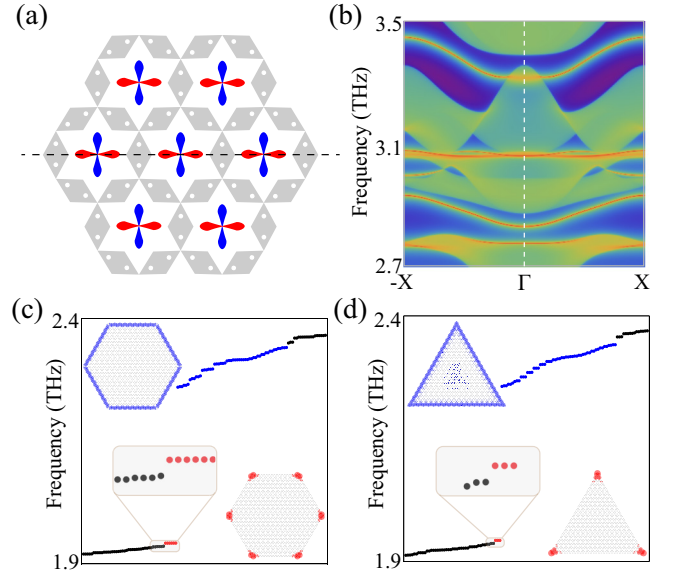
feOAI is [62]

$$\nexists N_{i,j} \geqslant 0, \quad \in \mathrm{N}, s.t. N_{Occ} = \sum_i^M \sum_j^{N_{rep,\omega_i}} d\left(\rho_{\omega_i}^j \uparrow G\right) N_{i,j}, \quad (1)$$

where N_{Occ} and $N_{i,j}$ are numbers of occupied bands and orbitals $(\rho_{\omega_i}^j \uparrow G)$, respectively. The parameter j sums over all of the occupied WPs, and $N_{i,j}$ are required to be a non-negative integer.

Now, we adopt the concept of feOAI to verify phonon band topology of MX_3, where the occupied WPs are 2c and 6k. The possible dimensions of Irrps that are induced from orbitals at these two WPs are $d(\rho_{2c}^j \uparrow G) = 2$ or 4, and $d(\rho_{6k}^j \uparrow G) = 6$. Thus, a necessary condition for MX_3 monolayers belonging to a conventional atomic insulator is $N_{Occ} = 2l$ with non-negative integer l. Equivalently, if a set of phonon branches whose BR is diagnosed as a sum of EBRs and the corresponding N_{Occ} is odd, this set of phonon branches may belong to the OAI. We note that the corresponding N_{Occ}s for the four visible band gaps in the phonon spectrum of BiI$_3$ monolayer [see Fig. 2(c)] are $N_{Occ} = 12, 13, 17$, and 21. Hence, except for the gap around 1.7 THz ($N_{Occ} = 12$), the other three band gaps are in the OAI phase. This is the reason for the emergence of the floating SS in Fig. 2(d). Meanwhile, the floating SSs are also observed when the $N_{Occ} = 17$ and 21, as shown in Fig. 3(b). Besides, the emergence of OAI phases also needs the appearance of band gaps. As shown in Table S3 of the SM [59], we list whether the band gaps are present at the odd N_{Occ} in the phonon spectra of all possible MX_3 candidates.

The results show that the OAI phase always occurs in the MX_3 monolayers.

To further confirm the OAI phase in the phonon of MX_3, based on the BR, we can get one $\mathbb{Z}$ type RSI and one $\mathbb{Z}_2$ type RSI with nonzero integers. The RSIs defined in real space at $1a$ and $6i$ are [28,59,63]

$$\delta_2(a) = -m(E_g) + m(E_u) = 1, \tag{2}$$

and

$$\eta_4(i) = [-m(A) + m(B)] \mod 2 = 1, \tag{3}$$

where the integer $m(\rho_{\omega_i}^j)$ means the multiplicity of Irrps $\rho_{\omega_i}^j$. The RSI $\delta_2(a) = \eta_4(i) = 1$ implies that there is at least one E_u and one A (or B) orbital pinned at unoccupied WPs $1a$ and $6i$, respectively. Thus, as an example, when the cleavage termination cuts through the black dashed line in Fig. 3(a), that is, the $1a$ or $6i$ position is exposed to the edge, the floating SSs can be present [see Figs. 2(d) and 3(b)]. For gaps with $N_{Occ} = 17$ and 21, as shown in the SM [59], we also get nonzero RSI, which indicates that these two gaps are also in the OAI phase. Notably, this HOTI phase is beyond the framework of real Chern insulators [59,64,65].

HOTIs with robust corner states.— It has been reported that the mismatch between the Wannier charge centers and the occupied WPs indicates the existence of higher-order band topology. As an essential feature, this mismatch is naturally satisfied in OAIs. Thus, we should have phonon corner modes appear in gaps of MX_3 since the phonon spectra of these monolayers are in the OAI phase. For instance, we consider the gap between PB_{13} and PB_{14}, i.e., that between 1.938 THz and 2.339 THz in the phonon spectrum of BiI_3. To directly show the corner states, we calculate the energy spectrum for a hexagonal-shaped nanodisk of BiI_3 that preserves C_{3z}, P, and M_{120} symmetries with open boundaries. As expected, we find that there are six degenerate modes at 1.943 THz and many nondegenerate modes emerge in the gap, as highlighted in red and blue in Fig. 3(c), respectively. The spatial distributions of six degenerate modes are symmetrically localized at the six corners of the nanodisk, indicating that these modes are phonon corner states. As a comparison, as plotted in blue in Fig. 3(c), the other modes in the gap are located at the six edges of the nanodisk, and thus they are the edge states. As shown in Fig. 3(d), the similar calculations are done for a triangular-shaped nanodisk where the inversion symmetry P is broken. We also obtain three degenerate modes at 1.943 THz corresponding to corner states. Therefore, we conclude that the phononic HOTI phase is indeed present in the BiI_3 monolayer. As discussed in the SM [59], we demonstrate that this HOTI phase is beyond the framework of real Chern insulators [64,65] where the corner modes are also reported.

For the MX_3 monolayers, the potentially exposed WPs are $1a$, $6i$, and $3f$, respectively. Remarkably, the RSIs defined at $3f$ are all zero, BR induced from A *orbital* at $6i$ is equivalent to that induced by putting A_g and A_u orbitals at $3f$, which indicates the $3f$ position also play as an effective OWCC. Thus, all of the potentially exposed WPs are occupied by OWCCs; the corner modes in MX_3 would be robust and independent of clipping forms or cleavage terminations of nanodisk geometries. To confirm this prediction,
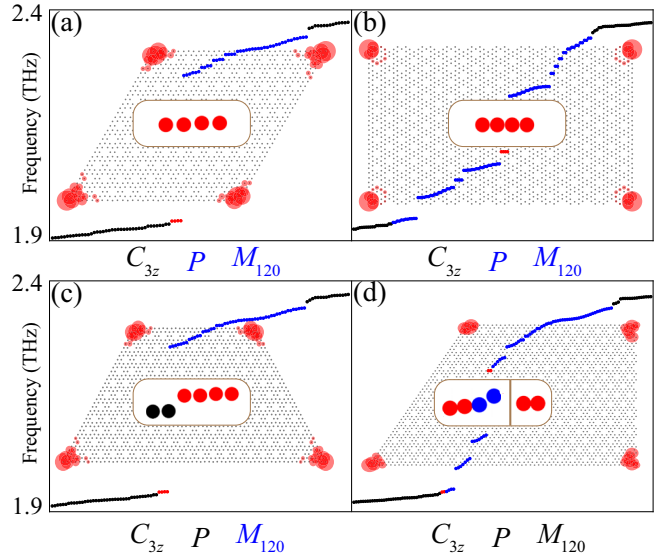

FIG. 4. (a)–(d) The computed spatial distributions of emerging corner states in the energy spectra for a (a) rhombic-, (b) rectangular-, (c) trapezoidal-, and (d) semi-trapezoidal-shaped nanodisks. The broken and maintained symmetries are marked by the text in black and blue, respectively. The corner, edge, and bulk states are marked in red, blue, and black, respectively. The spatial distribution of the corner modes are inserted.

we respectively compute the frequency spectra for rhombic-, rectangular-, trapezoidal-, and semi-trapezoidal-shaped nanodisks, as shown in Figs. 4(a)−4(d). The C_{3z} symmetry is broken in the rhombic- and rectangular-shaped nanodisks, and the C_{3z} and P (C_{3z}, P, and M_{120}) symmetries are broken in the trapezoidal-shaped (semi-trapezoidal-shaped) nanodisks. In these four different nanodisks, we can always find phonon corner modes in the gaps, and their spatial distributions localized at the corners are clearly visible. In the SM [59], we also revealed that the robustness of phonon corner states by investigating the energy spectrum of nanodisks with different cleavage terminations of atoms.

Summary.— In summary, using the theory of TQC, we established a scheme to realize robust corner states in 2D OAIs based an intuitive argument of how OWCCs locate at empty WPs. We emphasize that these corner states are independent of crystalline symmetries or terminated atoms of nanodisk geometries, exhibiting uniquely robust features of HOTI phases. Then, for the first time, we adopt the theory of TQC to diagnose phonon band topology and search phononic OAIs in 2D crystalline materials. We further show by firstprinciples calculations that the phononic OAIs with robust corner states can be realized in the 2D MX_3 monolayers. With the help of feOAI and RSI concepts, we proved that the gaps in the phonon spectra of MX_3 with odd occupied states are in the OAI phase. To verify these promising features of HOTIs, we obtained the phonon corner modes in different shapes or cleavage terminations of nanodisks. The robustness of corner states would facilitate to explore more attractive phenomena of higher-order band topology not only in phonon systems but also in electronic materials and artificial periodic systems, such as the As-Sb-As heterojunction in SM [59].

[1] W. A. Benalcazar, B. A. Bernevig, and T. L. Hughes, Quantized electric multipole insulators, Science **357**, 61 (2017).

[2] C. W. Peterson, W. A. Benalcazar, T. L. Hughes, and G. Bahl, A quantized microwave quadrupole insulator with topologically protected corner states, Nature (London) **555**, 346 (2018).

[3] F. Schindler, A. M. Cook, M. G. Vergniory, Z. Wang, S. S. Parkin, B. A. Bernevig, and T. Neupert, Higher-order topological insulators, Sci. Adv. **4**, eaat0346 (2018).

[4] Z. Song, Z. Fang, and C. Fang, $(d-2)$-dimensional Edge States of Rotation Symmetry Protected Topological States, Phys. Rev. Lett. **119**, 246402 (2017).

[5] J. Langbehn, Y. Peng, L. Trifunovic, F. von Oppen, and P. W. Brouwer, Reflection-Symmetric Second-Order Topological Insulators and Superconductors, Phys. Rev. Lett. **119**, 246401 (2017).

[6] E. Khalaf, Higher-order topological insulators and superconductors protected by inversion symmetry, Phys. Rev. B **97**, 205136 (2018).

[7] Z. Wang, B. J. Wieder, J. Li, B. Yan, and B. A. Bernevig, Higher-Order Topology, Monopole Nodal Lines, and the Origin of Large Fermi Arcs in Transition Metal Dichalcogenides XTe_2 ($X =$ Mo, W), Phys. Rev. Lett. **123**, 186401 (2019).

[8] W. A. Benalcazar, T. Li, and T. L. Hughes, Quantization of fractional corner charge in C_n-symmetric higher-order topological crystalline insulators, Phys. Rev. B **99**, 245151 (2019).

[9] Y. Xu, Z. Song, Z. Wang, H. Weng, and X. Dai, Higher-Order Topology of the Axion Insulator $EuIn_2As_2$, Phys. Rev. Lett. **122**, 256402 (2019).

[10] X.-L. Sheng, C. Chen, H. Liu, Z. Chen, Z.-M. Yu, Y. X. Zhao, and S. A. Yang, Two-Dimensional Second-Order Topological Insulator in Graphdiyne, Phys. Rev. Lett. **123**, 256402 (2019).

[11] R.-X. Zhang, F. Wu, and S. Das Sarma, Möbius Insulator and Higher-Order Topology in $MnBi_{2n}Te_{3n+1}$, Phys. Rev. Lett. **124**, 136407 (2020).

[12] C. Chen, Z. Song, J.-Z. Zhao, Z. Chen, Z.-M. Yu, X.-L. Sheng, and S. A. Yang, Universal Approach to Magnetic Second-Order Topological Insulator, Phys. Rev. Lett. **125**, 056402 (2020).

[13] H. Fan, B. Xia, L. Tong, S. Zheng, and D. Yu, Elastic Higher-Order Topological Insulator with Topologically Protected Corner States, Phys. Rev. Lett. **122**, 204301 (2019).

[14] X.-D. Chen, W.-M. Deng, F.-L. Shi, F.-L. Zhao, M. Chen, and J.-W. Dong, Direct Observation of Corner States in Second-Order Topological Photonic Crystal Slabs, Phys. Rev. Lett. **122**, 233902 (2019).

[15] E. Lee, R. Kim, J. Ahn, and B.-J. Yang, Two-dimensional higher-order topology in monolayer graphdiyne, npj Quantum Mater. **5**, 1 (2020).

[16] S. Qian, C.-C. Liu, and Y. Yao, Second-order topological insulator state in hexagonal lattices and its abundant material candidates, Phys. Rev. B **104**, 245427 (2021).

[17] H. Mu, B. Liu, T. Hu, and Z. Wang, Kekulé lattice in graphdiyne: Coexistence of phononic and electronic second-order topological insulator, Nano Lett. **22**, 1122 (2022).

[18] R. Gladstein Gladstone, M. Jung, and G. Shvets, Spin-Polarized Fractional Corner Charges and Their Photonic Realization, Phys. Rev. Lett. **128**, 026801 (2022).

[19] F. Schindler, M. Brzezińska, W. A. Benalcazar, M. Iraola, A. Bouhon, S. S. Tsirkin, M. G. Vergniory, and T. Neupert, Fractional corner charges in spin-orbit coupled crystals, Phys. Rev. Res. **1**, 033074 (2019).

[20] M. Proctor, P. A. Huidobro, B. Bradlyn, M. B. de Paz, M. G. Vergniory, D. Bercioux, and A. García-Etxarri, Robustness of topological corner modes in photonic crystals, Phys. Rev. Res. **2**, 042038 (2020).

[21] Y. Fang and J. Cano, Filling anomaly for general two- and three-dimensional C_4 symmetric lattices, Phys. Rev. B **103**, 165109 (2021).

[22] M. Z. Hasan and C. L. Kane, Colloquium: Topological insulators, Rev. Mod. Phys. **82**, 3045 (2010).

[23] H. Song, S.-J. Huang, L. Fu, and M. Hermele, Topological Phases Protected by Point Group Symmetry, Phys. Rev. X **7**, 011020(R) (2017).

[24] B. Bradlyn, L. Elcoro, J. Cano, M. Vergniory, Z. Wang, C. Felser, M. Aroyo, and B. A. Bernevig, Topological quantum chemistry, Nature (London) **547**, 298 (2017).

[25] S.-J. Huang, H. Song, Y.-P. Huang, and M. Hermele, Building crystalline topological phases from lower-dimensional states, Phys. Rev. B **96**, 205106 (2017).

[26] J. Cano, B. Bradlyn, Z. Wang, L. Elcoro, M. G. Vergniory, C. Felser, M. I. Aroyo, and B. A. Bernevig, Building blocks of topological quantum chemistry: Elementary band representations, Phys. Rev. B **97**, 035139 (2018).

[27] Z.-D. Song, L. Elcoro, and B. A. Bernevig, Twisted bulk-boundary correspondence of fragile topology, Science **367**, 794 (2020).

[28] Y. Xu, L. Elcoro, G. Li, Z.-D. Song, N. Regnault, Q. Yang, Y. Sun, S. Parkin, C. Felser, and B. A. Bernevig, Three-dimensional real space invariants, obstructed atomic insulators and a new principle for active catalytic sites, arXiv:2111.02433.

[29] J. Gao, Y. Qian, H. Jia, Z. Guo, Z. Fang, M. Liu, H. Weng, and Z. Wang, Unconventional materials: the mismatch between electronic charge centers and atomic positions, Sci. Bull. **67**, 598 (2022).

[30] Z. Guo, J. Deng, Y. Xie, and Z. Wang, Quadrupole topological insulators in $Ta_2M_3Te_5$ ($M =$ Ni, Pd) monolayers, npj Quantum Mater. **7**, 87 (2022).

[31] M. Ezawa, Higher-Order Topological Insulators and Semimetals on the Breathing Kagome and Pyrochlore Lattices, Phys. Rev. Lett. **120**, 026801 (2018).

[32] M. Ezawa, Topological Switch between Second-Order Topological Insulators and Topological Crystalline Insulators, Phys. Rev. Lett. **121**, 116801 (2018).

[33] R. Takahashi, T. Zhang, and S. Murakami, General corner charge formula in two-dimensional C_n-symmetric higher-order topological insulators, Phys. Rev. B **103**, 205123 (2021).

[34] L. Wang, Y. Jiang, J. Liu, S. Zhang, J. Li, P. Liu, Y. Sun, H. Weng, and X.-Q. Chen, Two-dimensional obstructed atomic insulators with fractional corner charge in MA_2Z_4 family, Phys. Rev. B **106**, 155144 (2022).

[35] M. Serra-Garcia, V. Peri, R. Süsstrunk, O. R. Bilal, T. Larsen, L. G. Villanueva, and S. D. Huber, Observation of a phononic quadrupole topological insulator, Nature (London) **555**, 342 (2018).

[36] S. Mittal, V. V. Orre, G. Zhu, M. A. Gorlach, A. Poddubny, and M. Hafezi, Photonic quadrupole topological phases, Nat. Photonics **13**, 692 (2019).

[37] A. El Hassan, F. K. Kunst, A. Moritz, G. Andler, E. J. Bergholtz, and M. Bourennane, Corner states of light in photonic waveguides, Nat. Photonics **13**, 697 (2019).

[38] B.-Y. Xie, G.-X. Su, H.-F. Wang, H. Su, X.-P. Shen, P. Zhan, M.-H. Lu, Z.-L. Wang, and Y.-F. Chen, Visualization of Higher-Order Topological Insulating Phases in Two-Dimensional Dielectric Photonic Crystals, Phys. Rev. Lett. **122**, 233903 (2019).

[39] G. Ma, M. Xiao, and C. T. Chan, Topological phases in acoustic and mechanical systems, Nat. Rev. Phys. **1**, 281 (2019).

[40] H. Xue, Y. Yang, F. Gao, Y. Chong, and B. Zhang, Acoustic higher-order topological insulator on a kagome lattice, Nat. Mater. **18**, 108 (2019).

[41] X. Ni, M. Weiner, A. Alu, and A. B. Khanikaev, Observation of higher-order topological acoustic states protected by generalized chiral symmetry, Nat. Mater. **18**, 113 (2019).

[42] Y. Qi, C. Qiu, M. Xiao, H. He, M. Ke, and Z. Liu, Acoustic Realization of Quadrupole Topological Insulators, Phys. Rev. Lett. **124**, 206601 (2020).

[43] S. Imhof, C. Berger, F. Bayer, J. Brehm, L. W. Molenkamp, T. Kiessling, F. Schindler, C. H. Lee, M. Greiter, T. Neupert *et al.*, Topolectrical-circuit realization of topological corner modes, Nat. Phys. **14**, 925 (2018).

[44] M. Ezawa, Higher-order topological electric circuits and topological corner resonance on the breathing kagome and pyrochlore lattices, Phys. Rev. B **98**, 201402(R) (2018).

[45] M. Serra-Garcia, R. Süsstrunk, and S. D. Huber, Observation of quadrupole transitions and edge mode topology in an lc circuit network, Phys. Rev. B **99**, 020304(R) (2019).

[46] L. Zhang, J. Ren, J.-S. Wang, and B. Li, Topological Nature of the Phonon Hall Effect, Phys. Rev. Lett. **105**, 225901 (2010).

[47] Y. Liu, C.-S. Lian, Y. Li, Y. Xu, and W. Duan, Pseudospins and Topological Effects of Phonons in a Kekulé Lattice, Phys. Rev. Lett. **119**, 255901 (2017).

[48] T. Zhang, Z. Song, A. Alexandradinata, H. Weng, C. Fang, L. Lu, and Z. Fang, Double-Weyl Phonons in Transition-Metal Monosilicides, Phys. Rev. Lett. **120**, 016401 (2018).

[49] H. Miao, T. T. Zhang, L. Wang, D. Meyers, A. H. Said, Y. L. Wang, Y. G. Shi, H. M. Weng, Z. Fang, and M. P. M. Dean, Observation of Double Weyl Phonons in Parity-Breaking FeSi, Phys. Rev. Lett. **121**, 035302 (2018).

[50] T. T. Zhang, H. Miao, Q. Wang, J. Q. Lin, Y. Cao, G. Fabbris, A. H. Said, X. Liu, H. C. Lei, Z. Fang, H. M. Weng, and M. P. M. Dean, Phononic Helical Nodal Lines with $\mathcal{PT}$ Protection in MoB_2, Phys. Rev. Lett. **123**, 245302 (2019).

[51] B. W. Xia, R. Wang, Z. J. Chen, Y. J. Zhao, and H. Xu, Symmetry-Protected Ideal Type-ii Weyl Phonons in CdTe, Phys. Rev. Lett. **123**, 065501 (2019).

[52] Y. Long, J. Ren, and H. Chen, Unsupervised Manifold Clustering of Topological Phononics, Phys. Rev. Lett. **124**, 185501 (2020).

[53] Y. Liu, X. Chen, and Y. Xu, Topological phononics: From fundamental models to real materials, Adv. Funct. Mater. **30**, 1904784 (2020).

[54] R. Wang, B. W. Xia, Z. J. Chen, B. B. Zheng, Y. J. Zhao, and H. Xu, Symmetry-Protected Topological Triangular Weyl Complex, Phys. Rev. Lett. **124**, 105303 (2020).

[55] J. Li, L. Wang, J. Liu, R. Li, Z. Zhang, and X.-Q. Chen, Topological phonons in graphene, Phys. Rev. B **101**, 081403(R) (2020).

[56] J. Li, J. Liu, S. A. Baronett, M. Liu, L. Wang, R. Li, Y. Chen, D. Li, Q. Zhu, and X.-Q. Chen, Computation and data driven discovery of topological phononic materials, Nat. Commun. **12**, 1204 (2021).

[57] J. Zhu, W. Wu, J. Zhao, C. Chen, Q. Wang, X.-L. Sheng, L. Zhang, Y. X. Zhao, and S. A. Yang, Phononic real chern insulator with protected corner modes in graphynes, Phys. Rev. B **105**, 085123 (2022).

[58] V. Peri, Z.-D. Song, B. A. Bernevig, and S. D. Huber, Fragile Topology and Flat-Band Superconductivity in the Strong-Coupling Regime, Phys. Rev. Lett. **126**, 027002 (2021).

[59] See Supplemental Material at http://link.aps.org/supplemental/10.1103/PhysRevB.108.L100101 for the details of calculations, lattice parameters for different MX_3 monolayers, the band representation of phonon spectrum of BiI_3, the effect of atomic terminal of nanodisk on the corner modes, the robust corner modes in fermionic systems, and the experimental realization of corner modes in phonons which includes Refs. [64,66–82].

[60] J. Li, X. Guan, C. Wang, H.-C. Cheng, R. Ai, K. Yao, P. Chen, Z. Zhang, X. Duan, and X. Duan, Synthesis of 2d layered BiI_3 nanoplates, BiI_3/WSe_2 van der waals heterostructures and their electronic, optoelectronic properties, Small **13**, 1701034 (2017).

[61] Z. Wang, A. Alexandradinata, R. J. Cava, and B. A. Bernevig, Hourglass fermions, Nature (London) **532**, 189 (2016).

[62] Y. Xu, L. Elcoro, Z.-D. Song, M. Vergniory, C. Felser, S. S. Parkin, N. Regnault, J. L. Mañes, and B. A. Bernevig, Filling-enforced obstructed atomic insulators, arXiv:2106.10276.

[63] The full definition of RSIs at different Wyckoff Positions of space group $P\bar{3}1m$ could be found at https://www.cryst.ehu.es/cgi-bin/cryst/programs/rsiindices.pl.

[64] Y. Zhao, Equivariant pt-symmetric real chern insulators, Front. Phys. **15**, 1 (2020).

[65] K. Wang, J.-X. Dai, L. B. Shao, S. A. Yang, and Y. X. Zhao, Boundary Criticality of $\mathcal{PT}$-Invariant Topology and Second-Order Nodal-Line Semimetals, Phys. Rev. Lett. **125**, 126403 (2020).

[66] W. Kohn and L. J. Sham, Self-consistent equations including exchange and correlation effects, Phys. Rev. **140**, A1133 (1965).

[67] G. Kresse and J. Furthmüller, Efficient iterative schemes for ab initio total-energy calculations using a plane-wave basis set, Phys. Rev. B **54**, 11169 (1996).

[68] G. Kresse and D. Joubert, From ultrasoft pseudopotentials to the projector augmented-wave method, Phys. Rev. B **59**, 1758 (1999).

[69] P. E. Blöchl, Projector augmented-wave method, Phys. Rev. B **50**, 17953 (1994).

[70] J. P. Perdew, K. Burke, and M. Ernzerhof, Generalized Gradient Approximation Made Simple, Phys. Rev. Lett. **77**, 3865 (1996).

[71] J. P. Perdew, K. Burke, and M. Ernzerhof, Generalized Gradient Approximation Made Simple [Phys. Rev. Lett. 77, 3865 (1996)], Phys. Rev. Lett. **78**, 1396 (1997).

[72] H. J. Monkhorst and J. D. Pack, Special points for brillouin-zone integrations, Phys. Rev. B **13**, 5188 (1976).

[73] A. Togo and I. Tanaka, First principles phonon calculations in materials science, Scr. Mater. **108**, 1 (2015).

[74] Z. Zhang, Z.-M. Yu, G.-B. Liu, and Y. Yao, A phonon irreducible representations calculator, arXiv:2201.11350.

[75] Q. Wu, S. Zhang, H.-F. Song, M. Troyer, and A. A. Soluyanov, Wanniertools: An open-source software package for novel topological materials, Comput. Phys. Commun. **224**, 405 (2018).

[76] B. McCollum, D. Dudis, A. Lachgar, and J. D. Corbett, The layered, metallic scandium iodide $Sc_{0.93}I_2$: Synthesis, structure, and properties, Inorg. Chem. **29**, 2030 (1990).

[77] M. I. de Barros Marques, M. A. Marques, and J. R. Rodrigues, The structure of the first coordination shell of the yttrium ion in concentrated aqueous solutions of YBr_3 and YCl_3, J. Phys.: Condens. Matter **4**, 7679 (1992).

[78] X.-P. Li, D.-S. Ma, C.-C. Liu, Z.-M. Yu, and Y. Yao, From atomic semimetal to topological nontrivial insulator, Phys. Rev. B **105**, 165135 (2022).

[79] X. Ding, X. Jin, Z. Chen, X. Lv, D.-S. Ma, X. Wu, and R. Wang, Abundant surface-semimetal phases in three-dimensional obstructed atomic insulators, Phys. Rev. B **108**, 085135 (2023).

[80] D. Templeton and G. F. Carter, The crystal structures of yttrium trichloride and similar compounds, J. Phys. Chem. **58**, 940 (1954).

[81] H. Fjellvåg and P. Karen, Crystal structure of $ScCl_3$, Acta Chem. Scand. **48**, 294 (1994).

[82] G. Srivastava, *The Physics of Phonons* (CRC, Boca Raton, FL, 1990).